International Journal of Plasticity 25 (2009) 1456–1473

Contents lists available at ScienceDirect

International Journal of Plasticity

journal homepage: www.elsevier.com/locate/ijplas

Multiscale modeling of the plasticity in an aluminum single crystal

S. Groh [a], E.B. Marin [a], M.F. Horstemeyer [a,*], H.M. Zbib [b]

[a] Center for Advanced Vehicular System, Mississippi State University, Box 5405, Mississippi State, MS 39762, USA
[b] School of Mechanical and Materials Engineering, Washington State University Pullman, WA, USA

ARTICLE INFO

Article history:
Received 9 April 2008
Received in final revised form 27 October 2008
Available online 27 November 2008

Keywords:
Multiscale modeling
A. Dislocations
B. Crystal plasticity
C. Finite element
B. Constitutive behavior

ABSTRACT

This paper describes a numerical, hierarchical multiscale modeling methodology involving two distinct bridges over three different length scales that predicts the work hardening of face centered cubic crystals in the absence of physical experiments. This methodology builds a clear bridging approach connecting nano-, micro- and meso-scales. In this methodology, molecular dynamics simulations (nanoscale) are performed to generate mobilities for dislocations. A discrete dislocations numerical tool (microscale) then uses the mobility data obtained from the molecular dynamics simulations to determine the work hardening. The second bridge occurs as the material parameters in a slip system hardening law employed in crystal plasticity models (mesoscale) are determined by the dislocation dynamics simulation results. The material parameters are computed using a correlation procedure based on both the functional form of the hardening law and the internal elastic stress/plastic shear strain fields computed from discrete dislocations. This multiscale bridging methodology was validated by using a crystal plasticity model to predict the mechanical response of an aluminum single crystal deformed under uniaxial compressive loading along the [421] direction. The computed strain-stress response agrees well with the experimental data.

1. Introduction

In the mid-1960s, Brown (1964), Bacon (1967) and Foreman (1967) established the framework to characterize the curvature of a line of dislocation under an applied stress. In the late 1970s, Kocks and

* Corresponding author.
E-mail address: mfhorst@cavs.msstate.edu (M.F. Horstemeyer).

0749-6419/$ - see front matter © 2008 Elsevier Ltd. All rights reserved.
doi:10.1016/j.ijplas.2008.11.003

Mecking (1979) proposed one of the first attempts of crystal plasticity models linking plasticity to microstructure (population of dislocations). Their model was physically-based and derived from the total dislocation density stored in a material. The associated assumptions included an unidirectional model, a homogeneous deformation state, and, if a polycrystal, all of the grains must be oriented along the same direction to have a homogenous plastic deformation. These dislocation-based studies, among others, played a part on the development of the Discrete Dislocation (DD) approach, a numerical tool based on linear elasticity that links the properties of a single dislocation to the collective behavior of dislocations (hardening), as proposed for two-dimensional problems by Amadeo and Ghoniem (1990) and Canova and Kubin (1991). As such, it is clear that the properties of a single dislocation can be linked to a dislocation-based Crystal Plasticity (CP) model using DD. Development of dislocation-based hardening rules has been pursued by many authors. Le and Stumpf (1996) presented an elastoplastic model that takes into account the motion of continuously distributed dislocations. Later, Langlois and Berveiller (2003) proposed a dislocation based model motivated from evolving microstructure for metals under monotonic and sequential loading. Hiratani et al. (2003) developed a model for thermally activated dislocation glide. Shizawa and Zbib (1999) proposed a thermodynamically-motivated theory of gradient elastoplasticity based on a dislocation density tensor, theory that was applied to model dislocation reactions between geometrically necessary dislocations (GNDs) and immobile dislocations (Shizawa and Zbib, 2001). Aoyagi and Shizawa (2007) developed a multiscale crystal plasticity model based on GND density and lattice incompatibility to establish a numerical method for fine-graining of a polycrystal. Shenoy et al. (2008) proposed a hierarchical multiscale framework linking a crystal plasticity model to a macroscopic internal state variable model. With their approach, the microstructure-dependence of the macroscale model parameters are identified at the crystal plasticity level.

The multiscale analysis presented in this work used as a basis the dislocation-based hardening model of Kocks and Mecking (2003), a model derived from the storage-recovery framework developed in scalar form by Kocks and Mecking (1979, 2003) and by Mecking and Estrin (1987). This model assumes that all the slip systems harden at the same rate and, therefore, the interactions between different slip systems are averaged in a Taylor sense. Extensions of this model to account for slip system interactions (matrix form) were carried out by Teodosiu et al. (1993). Within this extended storage-recovery framework, the hardening law was modified to predict the three stages behavior of a single crystal initially stretched in single slip (Tabourot et al., 1997; Fivel et al., 1998). The extended model predicted the main characteristics of single crystal and polycrystal deformation during monotonic and sequential loading tests. In this study, the interactions among the different slip systems were explicitly represented using an interaction coefficient matrix (Franciosi, 1985), where the value of the coefficients were extracted using DD simulations. Such extraction has been performed for fcc materials by Fivel (1997), Madec et al. (2003a,b) and Devincre et al. (2006), while for bcc materials in the athermal regime by Queyreau et al. (2008). Preußner et al. (2008) proposed a physics-based constitutive law, which allows describing the creep behavior of single crystal alloys by mutual interaction of dislocations on different slip systems, with an emphasis on the evolution of the dislocation density. Their model described well the first two stages of creep. A study related to the multiscale modeling of metals is presented by Ohashi et al. (2007), who used a multiscale modeling approach to model the scale-dependent characteristics of mechanical properties of metallic polycrystals. These authors proposed to modify the hardening law of a dislocation based crystal plasticity model (Ohashi, 1994) according to the minimum shear stress needed to emit a dislocation loop into a confined system calculated by DD simulations (Zbib and Diaz de la Rubia, 2002). Using such a multiscale approach, Ohashi et al. (2007) were able to reproduce a variation of the macroscopic yield stress as a function of the grain size.

The present work aims at describing a numerical multiscale framework connecting three disparate length scales (nano-, micro- and meso-scales) to determine the material parameters of a slip system hardening law expressed in a storage-recovery format. This hardening rule is then used in a crystal plasticity model to predict the deformation of an aluminum single crystal under uniaxial compression along the [421] direction. Validation experiments are available to assess the predictive capability of the approach. The presentation of the work is organized as follows. Section 2 gives the theoretical concept of the framework with an identification of the material parameters linking the different scales. Section 3 describes the simulation models used at each length scale to obtain the materials parame-

ters, while Section 4 presents the procedure to extract the value of those different parameters and a comparison to experimental data. Then, Section 5 gives a sensitivity study of the numerical results to the material parameters used by the flow rule. Finally, the last section states the concluding remarks.

2. Description of the hierarchical modeling approach

As the crystal plasticity model used in this study has already been presented previously (Marin and Dawson, 1998; Marin, 2006), this section mainly focuses on describing the flow rule and the hardening law employed in the model, the identification of the associated plasticity parameters, and the theoretical description of the method used to extract the hardening parameters from simulations at a lower length scale using DDs. Furthermore, this section also identifies the material parameters needed at the DD level and the corresponding methodology to calculate them at a lower length scale using Molecular Dynamics (MD).

At conventional 'quasi-static' strain rates, the localized obstacles to dislocation glide in fcc materials are mainly overcome by thermal activation. In such a case, the kinetics of dislocation motion is jerky, determined by the waiting time for thermal activation (Kocks et al., 1975). This description of the kinetics of dislocation motion (or the mean dislocation velocity) leads to a hyperbolic sine or exponential dependence on the resolved shear stress (Teodosiu and Sidoroff, 1976). If one assumes that the average dislocation velocity of each slip system follows the same law, the combination of the dislocation velocity equation given by Teodosiu and Sidoroff (1976) with Orowan's law produces a power law relationship for the kinetics of plastic flow on the α-slip system (Fivel, 1997),

$$\dot{\gamma}^{\alpha} = \dot{\gamma}_0 \left(\frac{\tau^{\alpha}}{\kappa^{\alpha}} \right)^{1/m} \tag{1}$$

Here, τ^{α} is the applied shear stress on the α-slip system, $\dot{\gamma}^{\alpha}$ is the shear strain rate, m is the strain rate sensitivity exponent, $\dot{\gamma}_0$ is a reference shear strain rate, and κ^{α} is the slip system strength or hardness. Using the theory of thermally activated glide, Fivel (1997) and Fivel et al. (1998) derived the strain rate sensitivity exponent and the reference shear rate as a function of temperature,

$$m = \frac{kT}{\alpha \mu b^2 d} \quad \text{and} \quad \dot{\gamma}_0 = \rho_m b^2 v_D \exp\left(\frac{-\Delta G_0}{kT} \right) \tag{2}$$

where k is the Boltzmann constant, T is the temperature, μ is the shear modulus, α is the average strength of the forest, b is the magnitude of the Burgers vector, d is a distance to bypass the obstacle, n_D is the Debye frequency, r_m is the density of mobile dislocations, and ΔG_0 is the energy stored in the material when an obstacle is bypassed by a dislocation. Typically, d is in the order of $4b$ while ΔG_0 is between $0.15\mu b^3$ and $0.25\mu b^3$. Also, at ambient temperature, m is approximately 0.005 and $\dot{\gamma}_0$ is between $10^{-16}\,s^{-1}$ and $10^{-6}\,s^{-1}$. For the numerical simulations presented in this work, the values of m and $\dot{\gamma}_0$ are increased in order to improve the numerical convergence during the integration of the crystal plasticity equations. Since in fcc materials the yield stress is not as strongly affected by the temperature as the hardening is, the strain rate sensitivity is artificially increased to 0.05 (Li, 2008). In addition, the reference strain rate is increased to the phenomenological value of $10^{-3}\,s^{-1}$. A sensitivity study of the predicted mechanical behavior from the multiscale methodology to the strain rate sensitivity and to the reference strain rate is presented in Section 5.

The specific form of the slip system hardening rule, which follows the hardening-recovery format proposed by Kocks and Mecking (2003), is developed assuming that all slip systems harden at the same rate (isotropic self-hardening), i.e., $\kappa^{\alpha} = \kappa$ for all α-slip systems. This assumption results in the following scalar form for the evolution law of κ (see Marin, 2006 for details)

$$\dot{\kappa}^{\alpha} = h_0 \left(\frac{\kappa_s - \kappa}{\kappa_s - \kappa_0} \right) \sum_{\alpha} |\dot{\gamma}^{\alpha}| \tag{3}$$

where κ_0 is the initial strength, κ_s is the saturation strength, and h_0 is the initial hardening rate. These parameters are characteristics of the material and describe its micro-structural properties. In essence, this hardening law assumes that hardening is mainly controlled by the competition of storage and anni-

hilation of statistically stored dislocations and its derivation implicitly assumes an average interaction among dislocations gliding on different slip systems. Note that latent hardening, i.e. the matrix form of the above evolution law, is not considered in this formulation. As such, with only self-hardening, the framework will mainly capture first-order hardening effects. Besides, this assumption also reduces the numerical computations with the crystal plasticity model as only one hardening equation needs to be integrated at each computational point. This hardening-recovery treatment of dislocation-based hardening has been well-established in the literature where Armstrong and Frederick (1966) first established the evolution of dislocation density in a hardening-recovery format. Later, Kocks (1970) and Bammann (1981, 1984) related the hardening-recovery equations to dislocation motion in an internal state variable context showing the temperature, strain rate, and path history effects. Many other crystal plasticity formulations employed such a formulation as well (c.f., Horstemeyer et al., 2005).

It is important to mention that Eqs. (1) and (3) rely on three main simplifications: (i) the interactions between moving dislocations and dislocation forest are the only mechanism for resistance to dislocation glide, (ii) a sufficient number of active slip system exist to allow uniform deformation, and (iii) there is no shortage of mobile dislocations. These assumptions are satisfied reasonably well by a pure FCC metal deformed under conditions in which there are no rapid changes in the deformation path (Estrin, 1996). These equations have been effectively employed to predict the deformed shape and the orientation changes in a fcc single crystal (Marin, 2006). Also, the scalar form of the hardening law has been successfully applied to predict the deformation of metals such as copper (Estrin and Mecking, 1984) and aluminum (Estrin, 1998).

In general, the material parameters in the hardening and flow rules are determined by correlating the model's predicted stress–strain response with experimental stress–strain curves. However, in this work we suggest that, in the absence of physical experiments, the present formulation can compute the material parameters of the hardening law, $(h_0, \kappa_s, \kappa_0)$, using a micro-scale approach based on DD simulations (Zbib et al., 1998; Ghoniem and Sun, 1999; Devincre et al., 2001; Madec et al., 2001). Discrete dislocation is a numerical technique where the plastic properties of a crystal are determined using the elastic theory of dislocations. Physically, plastic deformation in crystalline materials results from the collective interaction, motion, and reaction of a high density of dislocations. Since a dislocation is typically represented by a line singularity in an elastic solid (Volterra, 1907; Burgers, 1939), the evolution of the dislocation microstructure is governed by the elastic interactions between dislocations (Hirth and Lothe, 1982; Devincre, 1995). To model such evolution, the formulation of the DD approach assumes that the resolved shear stress τ^* on slip planes consists of various components: the Peach–Koehler force, τ^{PK}, the line tension, τ^{lt} and the Peierls force, τ^p,

$$\begin{cases} \tau^{**} = \tau^{pk} + \tau^{lt} \\ \tau^{*} = |\tau^{**}| - \tau^{p} \end{cases} \tag{4}$$

The stress due to the line tension corrects the energy due to the discrete nature of the framework, and the Peach–Koehler force includes the applied loading and the interaction between dislocations.

Once the resolved shear stress is calculated, the dislocation velocity is computed according to the mobility law, which, for a material with a low Peierls stress, can be written as (Nadgorny, 1998),

$$\begin{cases} v = 0, & \text{if} \quad \tau^* \leqslant 0 \\ v = \text{sign}(\tau^{**})\frac{\tau^* b}{B}, & \text{if} \quad \tau^* \leqslant 0 \end{cases}, \tag{5}$$

where B is the drag coefficient. Note that the linear dependence of the dislocation velocity on the resolved shear stress given by Eq. (5) represents the velocity of a single gliding dislocation and not the average velocity calculated over all dislocation gliding on one slip system. Also, the above equation for viscous glide applies to dislocation motion in pure fcc crystals when no interaction of the gliding dislocation with localized obstacles, e.g. forest dislocations, is considered. Then, depending on the temperature, the coefficient B accounts for electron and phonon drag. This is either the case of the free flight dislocation mobility between the obstacles at 'quasi-static' strain rates or the case of dislocation dynamics at high strain rates (Wang et al., 2007, 2009). Physically, as the dislocation velocity cannot exceed the terminal velocity, i.e. the velocity of a transverse shear wave, a resolved shear stress cut-off

value needs to be specified unless a complete dynamic analysis is used that includes an inertia term and an effective mass (Hirth et al., 1998). When the resolved shear stress becomes larger than the cut-off value, the dislocation velocity saturates at the terminal speed.

Once the velocity of the dislocation i is known, a search algorithm is applied to check if there are any possible interactions with other dislocations within a virtual area of the gliding dislocation i. The length of the dislocation segment and the free flight distance, $v_i \delta t$, define the virtual area gliding. The relation between the Burgers vector and the slip systems of the two intersecting dislocation segments define the type of interaction. When two dislocations intersect each other, one of the following interactions occurs:

- Annihilation, if the two dislocations have opposite Burgers vectors and glide in the same slip plane.
- Collinear annihilation, if the two dislocations have collinear Burgers vectors and glide in intersecting slip planes, each plane being the cross-slip plane of the other.
- Hirth lock, if the two dislocations have perpendicular Burgers vector and glide on different slip planes.
- Glissile junction, if the resulting Burgers vector is glissile on either of the planes.
- Lomer Lock, if the resulting Burgers vector is sessible on either of the planes.

Finally, internal stresses can relax by cross slipping of screw dislocations. A Monte Carlo method is used to check whether cross-slip is activated or not. The probability law of cross slip is given by

$$P = \beta \frac{L}{L_0} \frac{\delta t}{\delta t_0} \exp\left[-V \frac{\tau_{III} - \tau}{kT}\right] \tag{6}$$

where β is a coefficient that ensures that the probability does not exceed 1.0; $\tau_{III} = 5$ MPa is the critical resolved shear stress at the onset of Stage III work hardening for Al; $V_a = 300b^3$ is the activation volume; T is set to room temperature; $L_0 = 1$ μm and $\delta t_0 = 1$s are reference values of length and time, respectively; L is the length for cross slip of the screw dislocation segment; δt is the simulation time step; and τ is the resolved shear stress on the cross-slip plane (Kubin et al., 1992).

On the other hand, the increment of plastic shear is a consequence of the gliding of dislocation i of Burgers vector b_i and it is given by Orowan's law,

$$\delta \gamma_i^p = \frac{b_i \delta A_i}{V} \tag{7}$$

where $\mathrm{d}A_i$ is the area swept during gliding, and V is the volume of the sheared body. Knowing the increment of plastic shear on slip system k, one can then compute the components of the plastic strain rate tensor $\mathrm{d}\varepsilon_{ij}$ using

$$\delta \dot{\varepsilon}_{ij} = \sum_{k=1}^{12} \frac{1}{2} \left(n_i^{(k)} l_j^{(k)} + n_j^{(k)} l_i^{(k)} \right) \delta \dot{\gamma}^{(k)} \tag{8}$$

where $n_i^{(k)}$ and $l_i^{(k)}$ are the components of the unit vectors parallel to the slip plane normal and parallel to the Burgers vector, respectively. This framework associated with a set of periodic boundary conditions to equilibrate the flux of dislocations (Bulatov et al., 2001; Madec et al., 2003a,b) can be used to model the hardening response of a representative cell extracted from a single crystal. Note that some authors (e.g., Bulatov et al., 2001) showed that even with heterogeneous dislocation motion, periodic boundary conditions can appropriately represent the physical phenomena and as such they are used in this study.

As shown by Eq. (5), the drag coefficient B is an additional parameter introduced by the DD framework that needs to be computed by the multiscale approach. As expressed by this equation, this parameter is used to estimate the velocity of the dislocations as a function of the resolved shear stress. Such a law is usually given to describe the mobility of an infinite dislocation in a material with low lattice friction. In this work, the value of this parameter is computed using MD simulations (Daw

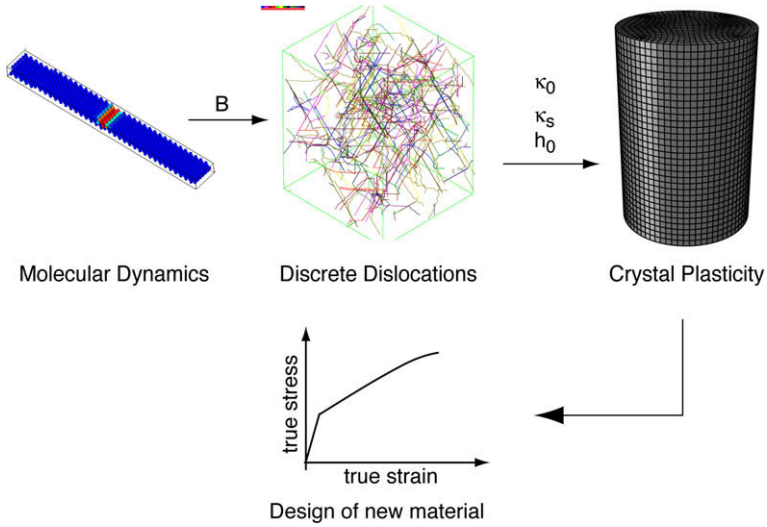

Fig. 1. A schematic showing a multiscale methodology that was used to calculate the material parameters of the hardening law needed at the crystal plasticity level to predict the mechanical response of a single crystal. The molecular dynamics, discrete dislocations and crystal plasticity models were involved to predict the mechanical response.

et al., 1993; Olmsted et al., 2005) for the motion of a single dislocation in a pure aluminum single crystal. The computed valued is then validated with the experimental data of Parameswaran et al. (1972).

The proposed multiscale methodology is illustrated in Fig. 1 which presents the three different length scales and corresponding simulation tools used to bridge the respective scales and predict the mechanical response of a single crystal of macroscale dimensions. Five material parameters are needed at the crystal plasticity level to numerically predict the strain-stress behavior. The two parameters of the flow rule can be estimated from published literature, while the three parameters in the hardening rule, i.e. h_0, κ_s and κ_0, can be calculated directly using DD simulations and then transferred hierarchically to the crystal plasticity level. At the DD level, the drag coefficient B needs to be quantified as well, either from experimental data or a lower length scale MD analysis. In this work, this coefficient is calculated numerically using MD and then transferred hierarchically to the DD level. The details of the simulation models used at the three different length scales are presented in the next section.

3. Simulation setup at the different length scales

This section summarizes the simulation models used at the different length scales in the multiscale approach. The proposed methodology was validated by predicting the stress–strain response and deformed shape of an aluminum single crystal compressed along the [4 2 1] axis, a case that was experimentally studied by Hughes et al. (2000). The *X*–*Y*–*Z* reference frame of the crystal was oriented along the $[2\,1\,\bar{1}\,\bar{0}]$, $[\bar{1}\,2\,0]$ and [4 2 1] crystal directions. Such deformation mode and crystal orientation led to dislocation glide on one primary slip system, altering during deformation the original shape of the crystal sample (right circular cylinder) to that of a cylinder with oval cross section with principal *X*–*Y*-axes. Microstructure studies of the experimentally deformed single crystals at large strains (60% of strain) revealed three levels of grain subdivision, including (i) long macroscale bands in a matrix structure, (ii) geometrically necessary boundary dislocations forming cellblocks, and (iii) dislocation cells (Hughes et al., 2000). Due to the numerical limitations of the DD framework, these different levels of subdivision were not investigated in this work. However, the formed dislocation microstructures generate backstresses, which give kinematic hardening at the macroscopic scale. Sauzay (2008)

proposed a model based on the Eshelby inclusion and the Berveiller and Zaoui (1979) approach to compute these intergranular backstresses.

3.1. Material parameter at the atomic scale

In metals characterized by a low Peierls stress such as Al phonon damping or drag is the main mechanism controlling the motion of both screw and edge dislocations. Although some MD studies (Olmsted et al., 2005) have shown that the drag coefficient of an edge dislocation was approximately two times smaller than that of a screw dislocation, the MD analysis in this work was only performed for the case of an edge dislocation. This should not affect the DD simulations as the velocity law given by Eq. (5) is mainly used as a "predictor" for the displacements of dislocation segments during the DD calculations.

As mentioned above, the drag coefficient (dislocation mobility) was quantified from MD simulations using a MEAM potential (Baskes, 1992; Jelinek et al., 2007) and the MD package WARP (Gullett et al., 2003). Compared to an EAM potential, the MEAM potential has the advantage of considering the angular force dependency, adding then additional parameters to setup the MEAM potential for an MD analysis. Using the MEAM potential, predictions of both the stacking fault energy and the elastic constants are in better agreement with experimental data (Jelinek et al., 2007). These two physical quantities typically control the dissociation of a full dislocation into two partials. Note that for high symmetry crystal structures, such as Al, the angular force dependency may not be too critical for the MD predictions, and hence, other atomistic potentials could have been used in this work without quantitatively affecting the numerical results.

For the simulations, the axes of the atomic specimen are oriented along the $[\bar{1}\,0\,1]$, $[\bar{1}\,\bar{1}\,\bar{1}]$, and $[1\,\bar{2}\,1]$ directions. The dimensions of the specimen are 17.86 nm by 11.22 nm by 1.73 nm. Dislocations are introduced in the form of a dipole so that the Burgers vector vanished using the procedure described in Chang et al. (1999). Periodic boundary conditions are applied along the line direction and the direction of dislocation motion. A shear stress is applied on the top and the bottom surfaces along the $[\bar{1}\,0\,1]$ direction with a time step of 1 fs. The temperature was isothermally controlled using a Nose-Hoover thermostat (Nose, 1984; Hoover, 1985). The dislocation core is located using the centrosymmetry value, and the dislocation velocity is then directly obtained as the dislocation glided on the slip plane. The dislocation motion occurred in three distinct stages: an initial transient stage, acceleration, and steady-state velocity (Mordehai et al., 2003). In this work, only the steady-state velocity is extracted from the MD calculation for a time ranging between 50 ps and 200 ps.

3.2. Material parameters at the dislocation dynamics level

Discrete dislocation simulations using the existing DD code (mM)[1] are performed to evaluate the material properties from Eq. (3). The simulation model includes the following features. The model crystal is a prismatic box (DD cell) with an initial microstructure consisting of a random distribution of Frank–Read loops over the 12 slip systems. As the long-range stress field of a loop varies as r^{-3}, no long-range stresses are generated using such an initial microstructure. The initial dislocation density is $10^{12}\ \mathrm{m}^{-2}$, to which a relaxation is applied to simulate annealed microstructures. Periodic boundary conditions are imposed in order to mimic a single crystal of infinite dimensions as the density of dislocations leaving and entering the unit cell is equilibrated. As the use of periodic boundary conditions in DD calculations can lead to self-annihilation of dislocation lines, a numerical artifact, the cell size must be such that the self-annihilation distance is larger than the dislocation mean free path. To satisfy this condition, the cell dimensions are calculated according to the method proposed by Madec et al. (2003a,b), resulting in a box with dimensions: 4.51 μm by 4.99 μm by 5.97 μm. With this cell size, no artificial length scale is introduced in the calculation, and hence, the dislocation mean-free path controls the dislocation microstructure development.

[1] "mM" is an open source code for DD simulations originaly developed at the Laboratoire d'Etude des Microstructures (CNRS-ONERA) and now available under the terms of the GNU GPL.

This dislocation box is deformed with a constant plastic strain rate of 20 s^{-1} applied along the [4 2 1] axis with a time step of 10^{-9} s. Reference mean lengths of 0.7 μm and 0.4 μm are used to force segment discretization on the active and inactive slip systems, respectively. Additional simulation conditions include the temperature at 300 K, the magnitude of the Burgers vector at 0.238 nm, and the elastic constants (Young modulus and Poisson's ratio) for Al. Note that, during the DD simulations, the number of dislocation segments increases drastically with deformation, and hence, to limit the CPU time, the DD analysis is limited to small deformations (less that 1%). Hence, the simulations do not account for the kinematics of large deformations.

3.3. Simulations at the crystal plasticity level

The numerical simulations at the meso-scale use a crystal plasticity model (Marin and Dawson, 1998; Marin, 2006) where the kinetics of plastic flow and dislocation hardening are mathematically represented by Eqs. (1) and (3), respectively. The particular application solved with this framework is the deformation analysis of an aluminum single crystal compressed along the [4 2 1] crystallographic direction. Experimental results are available to validate the predictions (Hughes et al., 2000). The material parameters used for the flow rule $(m, \dot{\gamma}_0)$ are estimated from the literature, while the hardening constants $(h_0, \kappa_s, \kappa_0)$ are computed numerically using DD. The anisotropic elastic constants (C_{11}, C_{12}, C_{44}) are those of Al.

Following the experimental work of Hughes et al. (2000), the single crystal is modeled as a right circular cylinder with dimensions 7.3 mm by 11 mm (diameter and height). The *x*-, *y*- and *z*-axes of the reference frame for the analysis are oriented along the crystal directions $[2\,1\,\overline{10}]$, $[\overline{1}\,2\,0]$ and [4 2 1], respectively. The cylinder is meshed with 14,976 brick finite elements, type ABAQUS-C3D8R (one integration point). The crystal is then deformed at room temperature under uniaxial compression along the *z*-axis ([4 2 1] crystal direction) by applying a variable negative displacement at the top of the cylinder such that a constant applied strain rate of 10^{-3} s^{-1} was obtained. The bottom of the cylinder has a zero *z*-displacement, with two points on this surface completely fixed to avoid rigid body motions. The lateral surface of the cylinder is stress free. The prescribed time interval and initial time step are $t = 600$ s and $\Delta t = 0.04$ s, respectively. During the solution, *ABAQUS* adjusts this time step in the range $\Delta t = 0.04$–4.0 s. The solution is obtained in 294 increments, with an average number of equilibrium iterations per increment of 3.

3.4. Bridging between the scales

In this work, both the time step and the boundary conditions are different at each length scales. For instance, the CP time step is approximately 10^{13} and 10^{7} times larger than the MD and DD time steps, respectively. Periodic boundary conditions are used for the MD and DD simulations, and uniaxial compression with the presence of free surfaces is considered for the CP calculations.

Scale bridging from MD to DD: The functional form between the dislocation velocity and the resolved shear stress is an input for the DD framework. Such a relationship depends on the material crystal structure. Therefore, for a FCC material, as the Peierls stress is low, a linear relationship between the dislocation velocity and the resolved shear stress is commonly assumed. The drag coefficient is an intrinsic material property, and it is independent of the boundary conditions including the strain rate. At the MD level, only the velocity of a pre-existing infinite dislocation was investigated, while the DD simulations were used to predict the behavior resulting for the collective motions and interactions of a large population of dislocations. For that reason, a time bridging between the MD and DD length scales is not warranted in this approach.

Scale bridging from DD to CP: The multiscale methodology presented in this work is developed to predict the stress–strain behavior of a pure Al single crystal of macroscale dimensions with the hardening predicted by DD as representative of the hardening of the single crystal. However, if the dimension of the specimen is drastically decreased, or if heterogeneities such as subgrain formation, inclusions, or cracks are taken into account, the presented methodology would require further modifications. Alternatively, concurrent multiscale methods (Van der Giessen and Needleman, 1995; Zbib

and Diaz de la Rubia, 2002; Weygand et al., 2002; Tang et al., 2006; El-Awady et al., 2008) could be used to address such issues.

4. Numerical results

4.1. Bridging the drag coefficient, B, from MD to DD

In FCC Al, the full $1/2[\bar{1}\,0\,1]a_0$ edge dislocation splits into two Shockley partials with a stacking fault region between them. According to elasticity theory, the dissociation length d_{sf} of an edge dislocation is obtained using the equation (Hirth and Lothe, 1982)

$$d_{sf} = \frac{\mu b^2}{24\pi\gamma_I}\frac{2+\nu}{1-\nu} \tag{9}$$

where γ_I is the stacking fault energy reported by Jelinek et al. (2007), b is Burgers vector length of the full dislocation, and ν is Poisson's ratio. In agreement with the elastic theory, which gives a separation length in the order of 1.66 nm, the MD calculations have shown a dissociation of the full edge dislocation into two partials separated by a distance of 1.43 nm.

Fig. 2a shows the evolution of the dislocation velocity for an edge dislocation of Burgers vector $[\bar{1}\,0\,1]$ as a function of the applied shear stress at a temperature of 300 K. The velocity is nearly linear in the resolved shear stress up to 100 MPa. Above 100 MPa, a transient regime is observed and the dislocation velocity smoothly converged to a saturation value, which is below the shear wave speed (3.32 nm/ps). This result agrees with the scaling predicted by phonon damping theory. As the Peierls stress can be neglected (Guyot and Dorn, 1967), in restricting the range of stresses from 0 to 100 MPa, one can correlate Eq. (5) to the dislocation velocity calculated by MD in order to quantify the drag coefficient. In varying the temperature between 100 and 500 K, the evolution of the drag coefficient as a function of the temperature can be predicted as displayed in Fig. 2b. This plot shows that the drag coefficient varies from 2.8×10^{-5} to 5.1×10^{-5} Pa s when the temperature increases from 100 to 500 K. Two lines with different slopes can be used to approximate the evolution of the drag coefficient as a function of the temperature. These two lines intersect each other at a temperature around 300 K (Nadgorny,1998); however, this temperature is lower than the one expected (the Debye temperature is close to 400 K in Al). Such a difference can be attributed to the underestimated value of the melting temperature calculated with the MEAM potential (Jelinek et al., 2007). Even with this Debye temper-

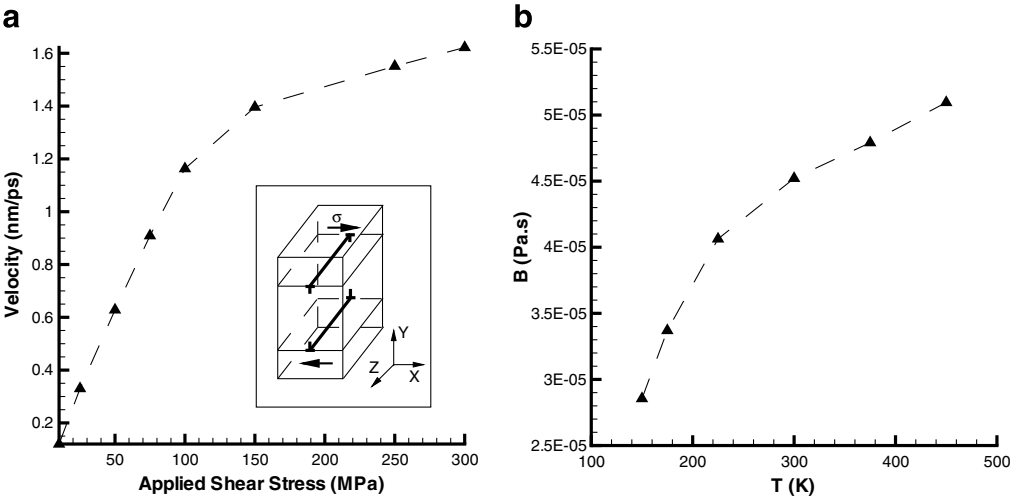

Fig. 2. (a) Velocity as a function of the applied shear stress for edge dislocations in Al. The inset figure represents the initial dipole configuration and the boundary conditions. (b) Dislocation damping constant vs. temperature.

ature difference, the obtained value of the drag coefficient agrees with the experimental values of Parameswaran et al. (1972) and close to the simulated damping constant of Olmsted et al. (2005) using an EAM potential.

Once the damping coefficient is calculated from MD simulations, its value is employed in Eq. (5) to model the time evolution of hardening using DD calculations in order to characterize the material parameters of the hardening law defined by Eq. (3).

4.2. Bridging the hardening parameters, h_0, κ_s and κ_0, from DD to crystal plasticity

Fig. 3 shows the evolution of the total plastic shear strain over the 12 slip systems as a function of time. The initial stage, up to $t = t_r$ ($t_r = 1.6 \times 10^{-5}$ s), corresponds to a relaxation of the initial configuration. For longer times, a linear regression can be used to determine the slope of the line defining the plastic shear strain rate. As the plastic deformation produced by the dislocation gliding must equilibrate the applied deformation, the plastic shear strain rate should be constant during the deformation test. The resolved plastic strain rate, which controls the load, is linked to the plastic shear strain rate according to

$$\dot{\varepsilon}_p = \sum_{k=1}^{12} S^{(k)} \dot{\gamma}^{(k)} \tag{10}$$

with $S^{(k)}$ being the Schmid factor of the slip plane (k). Therefore, the plastic shear strain rate of 41 s^{-1} obtained in Fig. 3 is in good agreement with the applied strain rate of 20 s^{-1}.

As the total plastic shear strain rates over the 12 slip systems is constant (Mecking and Kocks, 1981), Eq. (3) can be rewritten in the following form:

$$\dot{\kappa} = h_0 \left(\frac{\kappa_s - \kappa}{\kappa_s - \kappa_0} \right) C \tag{11}$$

where $C = \sum \dot{\gamma}^{\alpha}$ is the constant plastic shear strain rate calculated by DD, i.e. $C = 41$ s^{-1}. A closed form solution for the hardening as a function of the time was obtained by integrating Eq. (11) with respect to time between the limits $t = 0$ and t, which corresponded to the strength values of κ_0 and κ, respectively. The Palm–Voce equation (Palm, 1948; Voce, 1948) is then recovered,

$$\kappa = \kappa_s - (\kappa_s - \kappa_0) \exp\left(-\frac{h_0}{\kappa_s - \kappa_0} Ct \right) \tag{12}$$

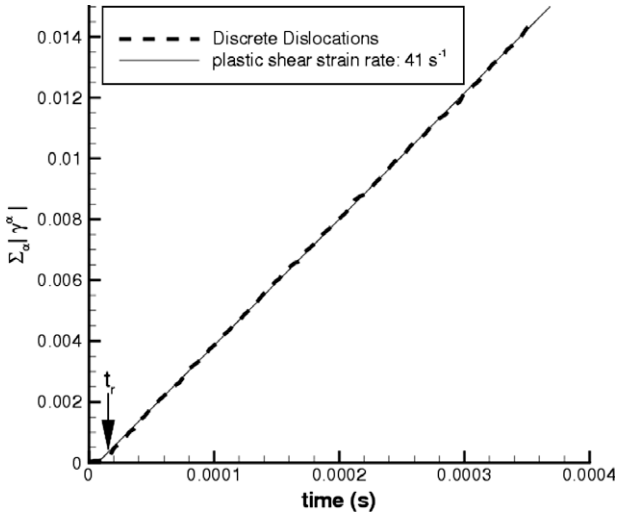

Fig. 3. Evolution of the plastic shear strain as a function of the time. t_r is the relaxation time. By linear regression, the plastic shear strain rate is 41 s^{-1}.

This equation, originally derived in a phenomenological manner, represents well the strain hardening behavior for a range of metallic materials. The material parameters in Eq. (12), κ_s, h_0, and κ_0, are obtained by correlating the predicted value with the hardening evolution determined by DD. As DD calculations start initially using a random distribution of Frank–Read loops, the beginning of the plastic deformation is not controlled by dislocation interactions. For this reason, the time range for the correlation procedure needs to be limited to the forest-hardening regime. In general, the dislocation hardening can be written using the classical Taylor relation

$$\kappa = \alpha \mu b \sqrt{\rho_f} \tag{13}$$

where ρ_f is the forest dislocation density, and α is a constant representing an average of the junction strength over all existing dislocation configurations. Typically, in the forest-hardening regime, α is in the range 0.35 ± 0.1 for a dislocation density close to 10^{12} m^{-2} (Saada, 1960; Madec, 2001).

The evolution of the α coefficient with time is plotted in Fig. 4. As noted from this figure, the time evolution of α can be decomposed into two distinct regions. The first region is for the time between 0 and t_0, where α increases from 0 to 0.7 and then decreases to the saturation value of 0.34. During this transient region, the initial microstructure of dislocations is reorganized, and the first Frank–Read loops activate. As such, in this region the hardening is not controlled by the interaction between dislocations. On the other hand, the second region corresponds to $t > t_0$ where α oscillated around an averaged value of 0.34. This value then indicates that, in this region, the interactions between dislocations control the hardening strength. Note that the observed oscillations of α can be attributed to the different time evolution of dislocation density on each slip system and, hence, the listed value of α is only an average value. Of course, taking the average value of α implies that the different types of interactions between dislocations are smeared out.

Because Eq. (12) models the hardening due to the storage/annihilation of dislocations, its correlation to the computed hardening from DD is then restricted to the region where the hardening is mainly controlled by dislocations interacting, i.e. the time interval $[t_0, \infty)$. Also, to study the effect of the initial time t_0 on the values of the hardening parameters, a shift δt_0 ranging from $\delta t_{0,1}$ to $\delta t_{0,2}$ is applied to t_0, meaning that the numerical correlation is performed for the time interval $[t_0 + \delta t_0, \infty)$. The results of this correlation are illustrated in Fig. 5, which presents both the time evolution of dislocation hardening predicted by DD, and the correlation of Eq. (12) for four different values

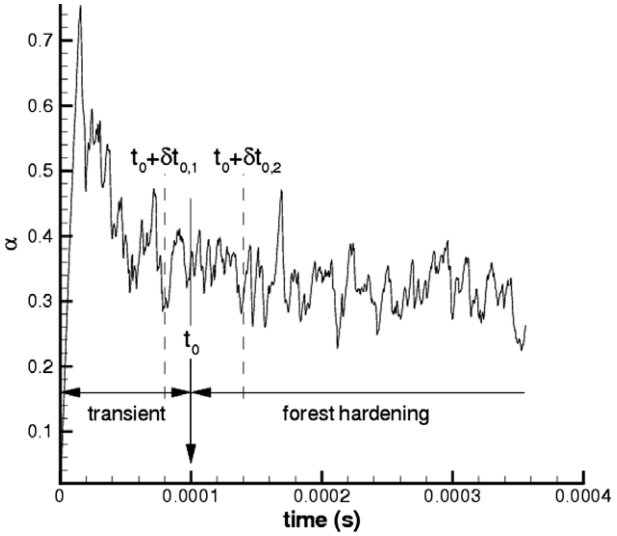

Fig. 4. Average value of the junction strength, α, as a function of the time. Below t_0, the interactions between dislocations do not control the hardening whereas above t_0, the interactions between dislocations control the hardening.

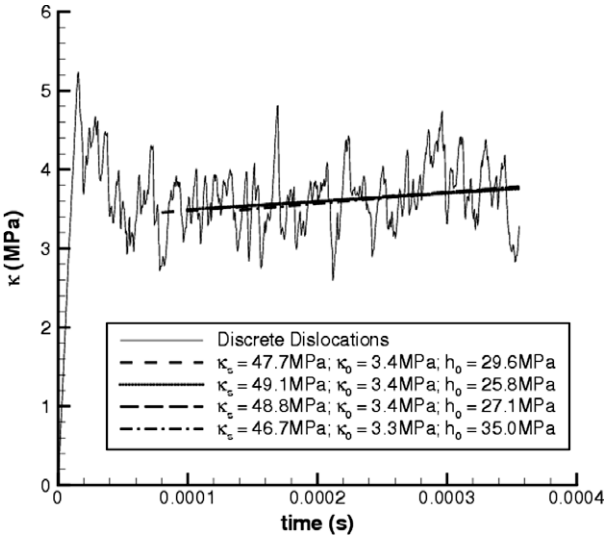

Fig. 5. Evolution of the hardening as a function of time modeled by dislocation dynamics. The dashed, dotted, long-dashed and dash-dot lines are plots of Eq. (8) with the materials parameters summarized in Table 1.

of δt_0: -2×10^{-5} s, 0 s, 2×10^{-5} s and 4×10^{-5} s. For each value of δt_0, the computed values of the saturation strength, κ_s, the initial strength, κ_0, and the initial hardening rate, h_0, are reported in Table 1.

As can be deduced from Table 1, the initial strength and the saturation strength are not very sensitive to the change in the value of t_0, as κ_0 changed from 3.29 to 3.36 MPa (2% increased), while κ_s varied from 46.75 MPa to 49.10 MPa (5% change). On the other hand, the initial hardening rate changes between 25.83 and 34.98 MPa (35% change) as t_0 is varied, showing then the highest sensitivity to variations in t_0. As these variations in the hardening parameters will affect the predicted hardening response, and hence, the computed stress–strain behavior in a crystal plasticity analysis, it is important to determine accurately the value of the time interval $[t_0, \infty)$. It is important to mention that there is some uncertainty in the computed value of κ_s, as the predicted hardening from DD is only restricted to short times (small deformation), and no numerical data at longer times is available. To account in part for this uncertainty, the fitting procedure was conducted for several initial guesses, and the values of κ_s reported in Table 1 are the ones leading to the minimum "chisquare" (the sum of squares of the residual). However, only numerical predictions of the hardening over a longer time using DD will help decrease the uncertainty on the value of κ_s.

4.3. Crystal plasticity simulations

Crystal plasticity calculations were carried out to predict the stress–strain response of an Al single crystal using the hardening parameters reported in Table 1. As mentioned before, the reference plastic shear strain rate and the strain rate sensitivity coefficient were set to the values of 10^{-3} s^{-1} and 0.05,

Table 1
Set of crystal plasticity material hardening parameters correlated from dislocation dynamics results.

DD set number	Time range (s) $\times 10^{-5}$	h_0 (MPa)	κ_0 (MPa)	κ_s (MPa)
1	0.08–0.4	29.6	3.4	47.7
2	0.10–0.4	25.8	3.4	49.1
3	0.12–0.4	27.1	3.4	48.8
4	0.14–0.4	35.0	3.3	46.7

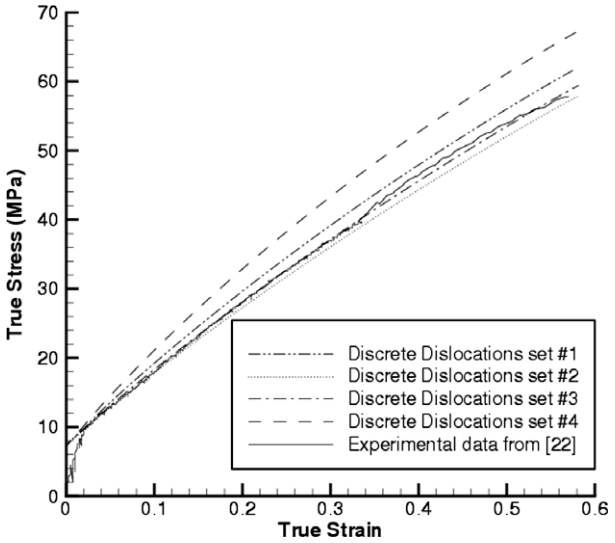

Fig. 6. Stress–strain response of single crystal under uniaxial compression along the [4 2 1] axis with a strain rate of $10^{-3}s^{-1}$. DD set #1–4 are obtained for the four different value of δt_0 -2×10^{-5} s, 0 s, 2×10^{-5} s and 4×10^{-5} s, respectively, and the corresponding value of h_0, κ_0 and κ_s are given in Table 1.

respectively. The effect of those two parameters on the mechanical behavior of Al single crystal is further elaborated in the next section.

The predicted stress–strain responses from the crystal plasticity model are plotted in Fig. 6 where, for comparison purposes, the experimental stress–strain curve taken from Hughes et al. (2000) is also presented. The stress tensor used to compute the effective stress was determined as the volume average of the stresses in all the elements. As shown by this figure, the predicted and the experimental mechanical responses were in good agreement, even though the hardening rate was higher with the Parameter Set #4 (time interval used for fitting the DD results: 0.14–0.4 ms, see Table 1). Also, the stress level after 60% of deformation for parameter sets #1 (58 MPa) and #2 (66 MPa) compared well with the experimentally determined value (58.5 MPa). Note that the elastic portion of the curve was not well captured, which may mean that the crystal elastic response determined from experiments was more compliant than the one predicted with the published values of the elasticity parameters.

The deformed mesh from the crystal plasticity simulation is illustrated in Fig. 7. Note that the crystal cross-section ovals during deformation. This geometric trend was also shown by the experimental results of Hughes et al. (2000) (see top of Fig. 7). In addition, the predicted lateral profile of the deformed mesh (along the oval major axis) reproduced the experimental shape (bottom of Fig. 7). However, this lateral profile was strongly affected by the strain rate sensitivity coefficient as presented in the next section.

5. Sensitivity of the simulated behavior to the parameters m and $\dot{\gamma}_0$

A simple sensitivity study was performed to determine the effect of the material parameters of the flow rule on both the stress–strain behavior and deformed shape of the Al single crystal. As the values of these parameters were assumed/determined from the open literature and, in general, they are not unique for a specific material, this sensitivity study will provide some insights of their effect on the deformation behavior of the Al single crystal selected in this work.

Fig. 8 presents the effect of the strain rate sensitivity exponent m on both the stress–strain response and the deformed shape at a strain of 60%. In these simulations, a reference strain rate of

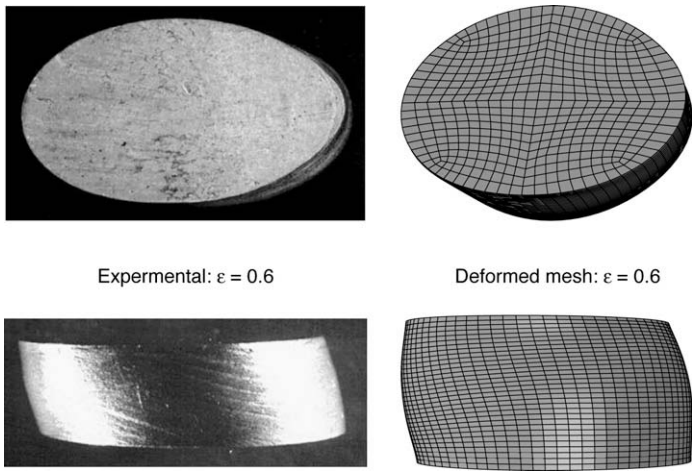

Fig. 7. Shape of the cylinder after 60% of deformation. Left: experimental data from Hughes et al. (2000). Right: simulated mesh using the set of parameters #2.

10^{-3} s^{-1} with the hardening parameters corresponding to set #2, Table 1. This figure shows that, for a strain lower than 20%, the stress–strain behavior was not affected by the value of m. However, as the deformation increased, the effect of m was noticeable. In particular, for the value of $m = 0.5$, the predicted curve deviated from the experimental one, having a decrease of 22 MPa at 60% strain.

In addition, Fig. 8 also shows that the shape of the deformed mesh was affected by the value of m. For the range between 0.05 and 0.25, the predicted deformed shape after 60% strain was in good agreement with the experimental one, whereas for low values of m, i.e. $m = 0.01$, the computed shape diverges from the experimental shape. In this case, a refined mesh did not improve the predictions.

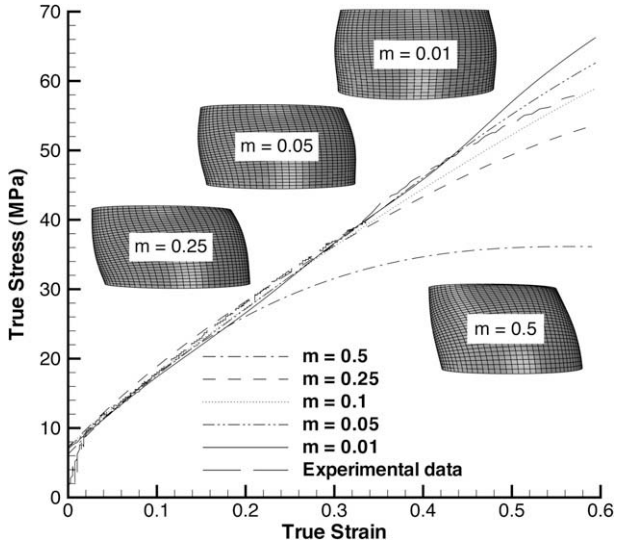

Fig. 8. Stress–strain response and corresponding deformed shape as a function of the strain rate sensitivity coefficient. The reference strain rate was setup to 10^{-3} s^{-1}.

Fig. 9a and b displays the evolution of the stress–strain response for the values of m of 0.05 and 0.25, respectively, each figure showing the curves computed with different values of the strain rate reference, ranging from 10^{-4} to 10^{-2} s^{-1}. Note that for $m = 0.05$, the stress level increased from 66 to 70 MPa when the strain rate reference was decreased from 10^{-2} to 10^{-4} s^{-1}, while, for $m = 0.25$, the stress level increased from 30 to 95 MPa as the reference strain rate decreased from 10^{-2} to 10^{-4} s^{-1}. On the other hand, the deformed shape was not affected when the strain rate reference was varied.

As a summary, Fig. 8 indicates that for a good prediction of the deformation behavior of the Al single crystal, the strain rate sensitivity exponent should be in the range between 0.05 and 0.25, and the strain rate reference should be set to 10^{-3} s^{-1}. Should the value referred by Alder and Phillips (1954) be used, then the upper bound used for the strain rate sensitivity coefficient needs to be decreased.

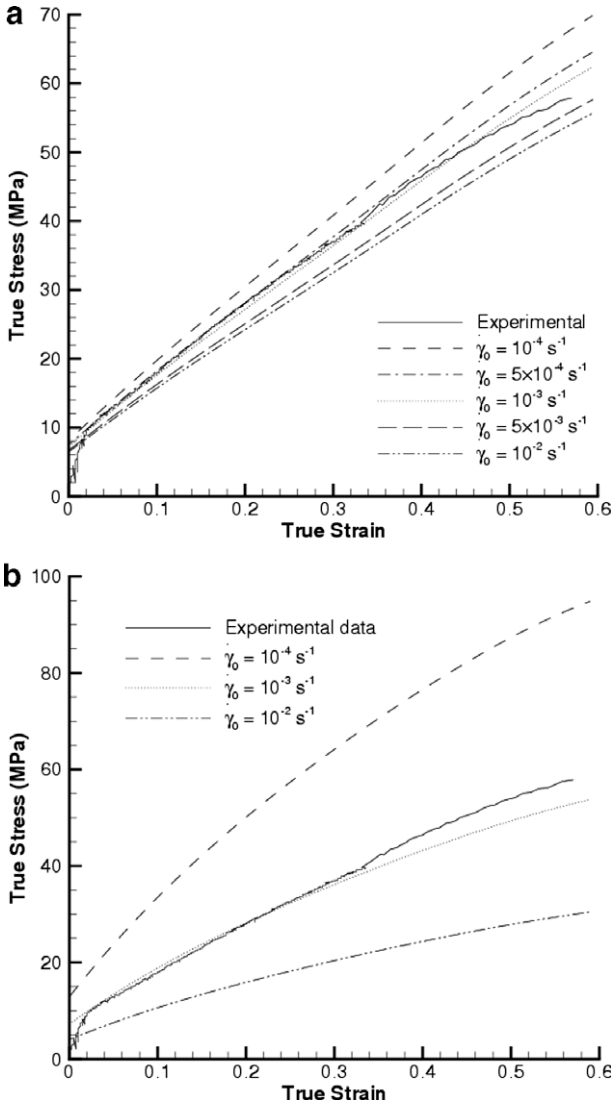

Fig. 9. Stress–strain response as a function of the reference strain rate. (a) $m = 0.05$ and (b) $m = 0.25$.

6. Concluding remarks

A multiscale materials modeling approach bridging the information passing between three distinct length scales was presented. Two bridging transitions were involved in this methodology: from molecular dynamics to discrete dislocations and then from discrete dislocations to crystal plasticity. The approach was used to determine the material parameters of a hardening law generally used in dislocation-based crystal plasticity models, and was applied to predict the deformation response of an aluminum single crystal under compression along the [421] crystallographic direction.

The approach computed the value of the drag coefficient at the MD level. Then, this coefficient was transferred to the DD level to simulate dislocation hardening. From the predicted hardening behavior, material parameters of the dislocation-based hardening law (initial strength, saturation strength, and initial hardening rate) were computed and transferred to the CP level. Due to the noisy evolution of hardening in the DD simulations, different starting points for the correlation of the material parameters were tested. Once the plastic deformation was controlled by the interaction between dislocations, the material parameters did not strongly depend of the lower bound defining the time range used for the correlation procedure.

The computed hardening parameters were then used in the CP framework to predict the mechanical response of an Al single crystal under compression. The simulated stress–strain behavior was in excellent agreement with the experimental data illustrating that this multiscale methodology is a good working theory to provide stress–strain behavior for metals upon further validation with other materials. An uncertainty of less than 10% from the experimentally determined stress was obtained after 60% of deformation. Note that hardening laws usually employ experiments to determine/calibrate the material constants. In this work, however, we used experiments to validate the parameters in the hardening law that were already determined from the multiscale methodology.

Acknowledgements

The authors are grateful to the Center for Advanced Vehicular Systems at Mississippi State University and to Oak Ridge National Laboratory for supporting this.

References

Alder, J.F., Phillips, V.A., 1954. Effect of strain rate and temperature on the resistance of aluminum, copper, and steel to compression. J. Inst. Met. 83, 80.

Amadeo, R., Ghoniem, N., 1990. Dislocation dynamics. I. A proposed methodology for deformation micromechanics. Phys. Rev. B 41, 6958–6967.

Aoyagi, Y., Shizawa, K., 2007. Multiscale crystal plasticity modeling based on geometrically necessary crystal defects and simulation on fine-graining for polycrystal. Int. J. Plasticity 23, 1022–1040.

Armstrong, P.J., Frederick, C.O., 1966. A mathematical representation of the multiaxial Bauschinger effect. CEGB Report RD/B/N731, Berkeley Nuclear Lab.

Bacon, D., 1967. A method for describing a flexible dislocation. Phys. Stat. Sol. 23, 527–538.

Bammann, D.J., 1984. An internal variable model of viscoplasticity. In: Aifantis, E.C., Davison, L. (Eds.), Media with Microstructures and Wage Propagation, International Journal of Engineering Science. Pergamon Press, Oxford. vols. 8–10, p. 1041.

Bammann, D.J., Aifantis, E., 1981. On the perfect lattice-dislocated state interaction. In: Selvadurai, A.P.S. (Ed.), Mechanics of Structured Media, Proceedings of the of International Symposium on Mechanical Behavior of Structured Media. Elsevier, Amsterdam.

Baskes, M., 1992. Modified embedded-atom potentials for cubic materials and impurities. Phys. Rev. B 46, 2727–2742.

Berveiller, M., Zaoui, A., 1979. An extension of the self-consistent scheme to plastically flowing polycrystals. J. Mech. Phys. Solids 26, 325–344.

Brown, L., 1964. The self-stress of dislocations and the shape of extended nodes. Philos. Mag. 10, 441–466.

Bulatov, V., Rhee, M., Cai, W., 2201. Periodic boundary conditions for dislocation dynamics simulations in three dimensions. In: Kubin, L.P., Bassani, J.L., Cho, K., Gao, H., Selinger, R.L.B. (M.M. of Materials Eds.), vol. 653, Mat. Res. Soc. Symp. Proc., 2001, pp. Z1.3.1–Z.1.3.6.

Burgers, J.M., 1939. Report of a conference of strength of solids. Proc. Kon. Ned. Acad. Wet. 47, 283–378.

Canova, G., Kubin, L., 1991. Dislocation microstructure and plastic flow: a three dimensional simulation. In: Maugin, G.A. (C. Model and D. Systems, Eds.), vol. 2, Longman Scientific and Technical, pp. 93–101.

Chang, J., Bulatov, V., Yip, S., 1999. Molecular dynamics study of edge dislocations motion in a bcc metal. J. Comput.-Aid Mater. Des. 6, 165–173.

Daw, M., Foiles, M., Baskes, S., 1993. The embedded-atom method: a review of theory and applications. Mater. Sci. Rep. 9, 251–310.
Devincre, B., 1995. Three-dimensional stress fields expressions for straight dislocation segments. Solid State Commun. 93, 875–878.
Devincre, B., Kubin, L., Lemarchand, C., Madec, R., 2001. Mesoscopic simulations of plastic deformation. Mater. Sci. Eng. A 309–310, 211–219.
Devincre, B., Kubin, L., Hoc, T., 2006. Physical analyses of crystal plasticity by DD simulations. Scripta Mater. 54, 741–746.
El-Awady, J.A., Biner, S.B., Ghoniem, N.M., 2008. A self-consistent boundary element, parametric dislocation dynamics formulation of plastic flow in finite volumes. J. Mech. Phys. Sol. 56, 2019–2035.
Estrin, Y., 1996. Dislocation-density-related constitutive modeling. In: Krausz, A.S., Krausz, K. (Eds.), Unified Constitutive Laws of Plastic Deformation. Academic Press, San Diego, pp. 69–110.
Estrin, Y., 1998. Dislocation theory based constitutive modelling: foundations and applications. J. Mater. Proc. Technol. 80–81, 33–39.
Estrin, Y., Mecking, H., 1984. A unified phenomenological description of work hardening and creep based on one-parameter models. Acta Metall. 32, 57–70.
Fivel, M., 1997. Etudes numériques à différentes échelles de la déformation plastique des monocristaux de structure CFC, Ph.D. Thesis, INPG/Université Joseph Fourier de Grenoble.
Fivel, M., Tabourot, L., Rauch, E., Canova, G., 1998. Identification through mesoscopic simulations of macroscopic parameters of physically based constitutive equations for the plastic behaviour of fcc single crystals. J. Phys. IV (Proc.) 8, 151–158.
Foreman, A., 1967. The bowing of a dislocation segment. Philos. Mag. 15, 1011–1021.
Franciosi, P., 1985. The concepts of latent hardening and strain hardening in metallic single crystals. Acta Metall. 33, 1601–1612.
Ghoniem, N., Sun, L., 1999. Fast-sum method for the elastic field of three-dimensional dislocation ensembles. Phys. Rev. B 60, 128–140.
Gullett, P.M., Wagner, G., Slepoy, A., Horstemeyer, M.F., Potirniche, G., Baskes, M.I., 2003. Numerical tools for atomistic simulation, Sandia National Laboratories Report, CA, SAND2003-8782.
Guyot, P., Dorn, J.E., 1967. A critical review on the Peierls mechanism. Can. J. Phys. 45, 983–1016.
Hiratani, M., Zbib, H.M., Khaleel, M.A., 2003. Modeling of thermally activated dislocation glide and plastic flow through local obstacles. Int. J. Plasticity 19, 1271–1296.
Hirth, J., Lothe, J., 1982. Theory of Dislocations, second ed. Wiley, New York.
Hirth, J.P., Zbib, H.M., Lothe, J., 1998. Forces on high velocity dislocations. Model. Simul. Mater. Sci. Eng. 6, 165–169.
Hoover, W.G., 1985. Canonical dynamics: equilibrium phase-space distributions. Phys. Rev. A 31, 1695–1697.
Horstemeyer, M.F., Potirniche, G., Marin, E.B., 2005. In: Yip, S. (Ed.), Mesoscale-Macroscale Continuum Modeling: Crystal Plasticity, Handbook for Materials Modeling. Springer, AA Dordrecht, The Netherlands. p. 3300 (Chapter 3).
Hughes, D., Bammann, D., Codfrey, A., Prantil, V., Holm, E., Miodownik, M., Chrzan, D. Lusk, M., 2000. Capturing recrystallization of metals with a multi-scale materials model, Sandia National Laboratories Report, CA, SAND2000-8232.
Jelinek, B., Houze, J., Kim, S., Horstemeyer, M.F., Baskes, M.I., Kim, S.-G., 2007. Modified embedded-atom method interatomic potentials for the Mg–Al alloy system. Phys. Rev. B 75, 054106.
Kocks, U.F., 1970. The relation between polycrystal deformation and single-crystal deformation. Metall. Mater. Trans. B 1, 1121–1143.
Kocks, U.F., Mecking, H., 1979. A Mechanism for Static and Dynamic Recovery. In Strength of Metals and Alloys. Pergamon Press, Oxford.
Kocks, U.F., Mecking, H., 2003. Physics and phenomenology of strain hardening: the fcc case. Prog. Mater. Sci. 48, 171–273.
Kocks, U.F., Argon, A.S., Ashby, M.F., 1975. Thermodynamics and Kinetics of Slip. Pergamon Press, Oxford.
Kubin, L., Canova, G., Condat, M., Devincre, B., Pontikis, V., Brechet, Y., 1992. Dislocation structures and plastic flow: a 3D simulation. Solid State Phenom. 23–24, 455–472.
Langlois, L., Berveiller, M., 2003. Overall softening and anisotropy related with the formation and evolution of dislocation cell structures. Int. J. Plasticity 19, 599–624.
Le, K.C., Stumpf, H., 1996. A model of elastoplastic bodies with continuously distributed dislocations. Int. J. Plasticity 12, 611–627.
Li, S., 2008. Orientation stability in equal channel angular extrusion. Part I. Face-centered cubic and body-centered cubic materials. Acta Mat. 56, 1018–1030.
Madec, R., 2001. Dislocation interactions to plastic flow in fcc single crystals: A study by simulation of dislocation dynamics, Ph.D. Thesis, Orsay University.
Madec, R., Devincre, B., Kubin, L., 2001. New line model for optimized dislocation dynamics simulations. In: Kubin, L.P., Bassani, J.L., Cho, K., Selinger, R.L.B. (M. Materials Modeling, Eds.), Mat. Res. Soc. Symp. Proc. vol. 653, 2001, pp. Z1.8.1–Z1.8.6.
Madec, R., Devincre, B., Kubin, L., 2003. On the use of periodic boundary conditions in dislocation dynamics simulations. In: Kitagawa, Y., Shibutani, H. (Eds.), Mesoscopic Dynamics in Fracture Process and Strength of Materials: IUTAM Symposium. Kluwer Academic Publisher, Dordrecht.
Madec, R., Devincre, B., Kubin, L., Hoc, T., Rodney, D., 2003a. The role of collinear interaction in dislocation-induced hardening. Science 301, 1879–1882.
Marin, E.B., 2006. On the formulation of a crystal plasticity model, Sandia National Laboratories, CA, SAND2006-4170.
Marin, E.B., Dawson, P.R., 1998. On modeling the elasto-viscoplastic response of metals using polycrystal plasticity. Comput. Methods Appl. Mech. Engrg. 165, 1–21.
Mecking, H., Estrin, Y., 1987. Microstructure related constitutive modelling of plastic deformation. In: 8th International Symposium on Metallurgy and Material Science, Riso, Denmark.
Mecking, H., Kocks, U., 1981. Kinetics of flow and strain hardening. Acta Metall. 29, 1865–1875.
Mordehai, D., Ashkenazy, Y., Kelson, I., 2003. Dynamic properties of screw dislocations in Cu: a molecular dynamics study. Phys. Rev. B 67, 024112-1–024112-8.
Nadgorny, E., 1998. Dislocation dynamics and mechanical properties. Progress in Materials Science 31. Pergamon Press, Oxford.
Nose, S., 1984. A molecular dynamics method for simulations in the canonical ensemble. Mol. Phys. 50, 255–268.

Ohashi, T., 1994. Numerical modeling of plastic multislip in metal crystals of fcc type. Philos. Mag. A 70 (5), 793–803.
Ohashi, T., Kawamukai, M., Zbib, H., 2007. A multiscale approach for modeling scale-dependent yield stress in polycrystalline metals. Int. J. Plasticity 23, 897–914.
Olmsted, S., Hector, J.L., Curtin, W., Clifton, R., 2005. Atomistic simulations of dislocation mobility in Al, Ni and Al/Mg alloys. Model. Simul. Mater. Sci. Eng. 13, 371–388.
Palm, J., 1948. Stress–strain relation for uniaxial loading. Appl. Sci. Rets. Sect. A 1, 198–210.
Parameswaran, V., Urabe, N., Weertman, V., 1972. Dislocation mobility in aluminium. J. Appl. Phys. 43, 2982–2986.
Preußner, J., Rudnik, Y., Brehm, H., Völkl, R., Glatzel, U., 2008. A dislocation density based material model to simulate the anisotropic creep behavior of single-phase and two-phase single crystals. Int. J. Plasticity. doi:10.1016/j.ijplas.2008.04.006.
Queyreau, S., Monnet, G., Devincre, B., 2008. Slip systems interactions in α-iron determined by dislocation dynamics simulations. Int. J. Plasticity. doi:10.1016/j.ijplas.2007.12.009.
Saada, G., 1960. Sur le durcissement dû à la recombinaison des dislocations. Acta Metall. 8, 841–847.
Sauzay, M., 2008. Analytical modeling of intergranular backstresses due to deformation induced dislocation microstructures. Int. J. Plasticity 24, 727–745.
Shenoy, M., Tjiptowidjojo, Y., McDowell, D., 2008. Microstructure-sensitive modeling of polycrystalline IN 100. Int. J. Plasticity 24, 1694–1730.
Shizawa, K., Zbib, H.M., 1999. A thermodynamical theory of gradient elastoplasticity with dislocation density tensor. Int. J. Plasticity 15, 899–938.
Shizawa, K., Zbib, H.M., 2001. A strain-gradient thermodynamical theory of plasticity based on dislocation density and incompatibility tensors. Mater. Sci. Eng. A 309–310, 416–419.
Tabourot, L., Fivel, M., Rauch, E., 1997. Generalised constitutive laws for fcc single crystal. Mater. Sci. Eng. A 234–236, 639–642.
Tang, M., Cai, W., Xu, G., Bulatov, V.V., 2006. A hybrid method for computing forces on curved dislocations intersecting free surfaces in three-dimensional dislocation dynamics. Model. Simul. Mater. Sci. Eng. 14, 1139–1151.
Teodosiu, C., Sidoroff, F., 1976. A finite theory of the elasto-viscoplasticity of single crystals. Int. J. Eng. Sci. 14, 713–723.
Teodosiu, C., Raphanel, J., Tabourot, L., 1993. Finite implementation of the large elastoplastic deformation of multicrystals. In: Teodosiu, C., Raphanel, J., Sidoroff, F. (Eds.), Large Plastic Deformation, pp. 153-168.
Van der Giessen, E., Needleman, A., 1995. Discrete dislocation plasticity: a simple planar model. Model. Simul. Mater. Sci. Eng. 3, 689–735.
Voce, E., 1948. The relation between stress and strain for homogeneous deformation. J. Inst. Met. 74, 537–562.
Volterra, V., 1907. Sur l'equilibre des corps elastiques multiplement connexes. Ann. Ecole Nom. Sup. 24, 400.
Wang, Z.Q., Beyerlein, I.J., LeSar, R., 2007. The importance of cross-slip in high rate deformation. Model. Simul. Mater. Sci. Eng. 15, 675–690.
Wang, Z.Q., Beyerlein, I.J., LeSar, R., 2009. Plastic anisotropy in fcc single crystal in high rate deformation. Int. J. Plasticity 25, 26–48.
Weygand, D., Friedman, L.H., Van der Giessen, E., Needleman, A., 2002. Aspects of boundary-value problem solutions with three-dimensional dislocation dynamics. Model. Simul. Mater. Sci. Eng. 10, 437–468.
Zbib, H.M., Diaz de la Rubia, T., 2002. A multiscale model of plasticity. Int. J. Plasticity 18, 1133–1163.
Zbib, H., Rhee, M., Hirth, J., 1998. On plastic deformation and the dynamics of 3D dislocation. J. Mech. Sci. 40, 113–127.